A SIMPLIFIED MODEL FOR SIZING AND CHARACTERIZING A NATURAL CONVECTION HEAT EXCHANGER SYSTEM

Nicholas Cramp[1] Stephen J. Harrison[2]
[1,2]Solar Calorimetry Laboratory, Department of Mechanical and Materials Engineering
Queen's University, Kingston Ontario, Canada
nick.cramp@queensu.ca harrison@me.queensu.ca

ABSTRACT

Natural convection heat exchangers have applications in heat pumps and solar domestic hot water (SDHW) systems due to their minimalist and low cost design. A simplified design tool was created to aid system designers in sizing and predicting the performance of a brazed plate heat exchanger (BPHE) as it charges a hot water storage tank via a natural convection flow. The program was designed in Microsoft Excel for ease of use and distribution, and applies iterative solutions built around Visual Basic algorithms. Previously, a complete system needed to be constructed and tested to characterize a specific configuration. The program allows the end user to specify their unique system geometry and components, in order to compare the effects of friction losses, pressure drops, and heat exchanger types. The program results can be used to identify critical design limitations which can increase both the performance and efficiency of a configuration.

INTRODUCTION

Driven by an ever increasing need for renewable energy sources, solar thermal production reached a worldwide production capacity of 374.7 GW_{th} by the end of 2013 [1]. One of the most common applications of solar thermal energy are solar domestic hot water systems (SDHW). These systems use electric pumps to circulate fluid through a collector plate and into a hot water storage tank for domestic use. In temperate climates, a non-toxic antifreeze solution is used in the collector loop, thus requiring a heat exchanger to transfer the thermal energy to a potable hot water storage tank. Compact brazed-plate heat exchangers (BPHE) are often used due to their large heat transfer surface areas and design simplicity. These systems have been optimized to eliminate the need for an electric pump on the storage side, relying instead on a buoyancy-driven natural convection thermosiphon [2]. This arrangement greatly simplifies the componentry required in a SDHW system (Fig.1).

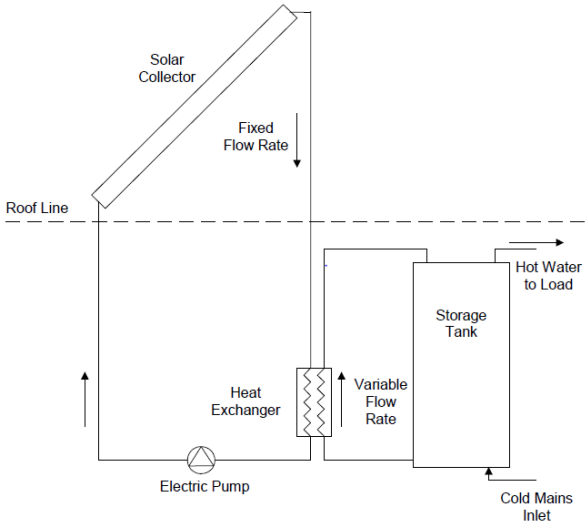

Fig. 1: Schematic of simple SDHW system with external heat exchanger.

With inherently low thermosiphon flowrates, stratified layers of hot water will form within the storage tank. Stratification has been shown to increase overall system performance by delivering water near the desired set-point temperature earlier in the charge cycle by avoiding mixing of the storage water [3]. The induced natural convection flowrate is dependent on the pressure head of the system, a function of the fluid density in the storage tank, and the total pressure loss across the system due to the componentry and plumbing used.

In the present study, this pressure dependency was investigated and used as a basis to develop a simplified model for determining the performance of a natural convection heat exchanger (NCHE) system. Developed in an easily distributable Microsoft Excel platform, the model was designed to allow system designers to size and characterize the performance of a SDHW system without physical construction or laborious testing.

METHODOLOGY

The performance of forced flow heat exchangers has

been thoroughly studied, with heat exchangers being characterized by their effectiveness (ε), capacity ratio (C_r), and the total number of heat transfer units ($NTU's$). For a natural convection flow the method used by Fraser et al. [4] was adopted which characterizes the heat exchangers using modified performance indices. These indices are based on the forced side capacitance rate, rather than the minimum capacitance rate. Replacing the minimum capacitance rate, $(\dot{m}c_p)_{min}$, with the forced capacitance rate, $(\dot{m}c_p)_c$, eliminates the case in which the convective mass flow rates drops to near zero, causing the effectiveness to approach infinity. These modified indices are defined in Eq. 1 to Eq. 3, where T_{so} is the storage side outlet temperature, T_{si} is the storage side inlet temperature, and T_{ci} is the inlet temperature of the water entering the heat exchanger from the solar collectors.

$$\varepsilon_{mod} = \frac{Q_{actual}}{Q_c} = \frac{(\dot{m}c_p)_s(T_{so} - T_{si})}{(\dot{m}c_p)_c(T_{ci} - T_{si})} \quad (1)$$

$$C_{r_{mod}} = \frac{(\dot{m}c_p)_s}{(\dot{m}c_p)_c} \quad (2)$$

$$NTU_{mod} = \frac{UA}{(\dot{m}c_p)_c} \quad (3)$$

Using these indices it has been shown that a specific heat exchanger can be characterized by two key relationships; the relationship between the pressure head and thermosiphon flow rate, and the relationship between the modified effectiveness and modified capacity ratio [5]. These relationships are given in Eq. 4 and Eq. 5 where $\dot{m}_s$ is the storage-side natural convection flow rate, ΔP_{hx} is the pressure loss across the heat exchanger, and a, b, c, and d are constants that are derived through experimental analysis for a specific heat exchanger.

$$\dot{m}_s = a * (\Delta P_{hx})^b \quad (4)$$

$$\varepsilon = c * C_{r_{mod}}^2 + d * C_{r_{mod}} \quad (5)$$

To model a NCHE system, critical information is required to determine the net hydrostatic pressure across the heat exchanger loop, i.e., the driving force of the thermosiphon. The pressure head is dependent on the difference in density of the fluid exiting the heat exchanger compared to the average density of the fluid within the storage tank (Eq. 6 and Eq. 7) [6].

$$\Delta P_{net} = \rho_{T_{tank}} g H_{tank} - \rho_{T_{so}} g H_{pipe} - \rho_{T_{hx}} g H_{hx} \quad (6)$$

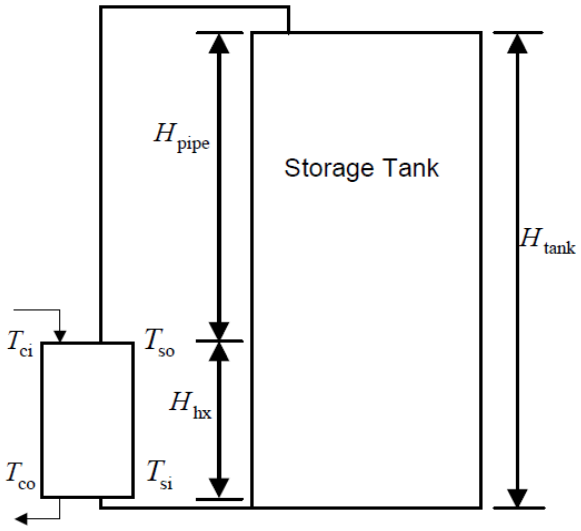

Fig. 2: Diagram of heat exchanger and tank configuration.

$$\Delta P_{net} = \rho_{T_{tank}} g H_{tank} - \rho_{T_{so}} g \left(H_{tank} - \frac{H_{hx}}{2}\right) - \rho_{T_{si}} g \frac{H_{hx}}{2} \quad (7)$$

$\rho_{T_{tank}}$ is the average tank density, $\rho_{T_{so}}$ is the density of the fluid exiting the heat exchanger on the storage side, and $\rho_{T_{si}}$ is the density of the fluid entering the heat exchanger on the storage side. The tank height, H_{tank}, and heat exchanger height, H_{hx}, are outlined in Fig. 2. It is imperative that the system be arranged in this fashion, with the heat exchanger base in line with the base of the tank.

At the beginning of the charging process, the natural convection flow rate will drop dramatically over a short time period due to the large quantities of hot water entering the tank. As the average tank temperature increases, the flow rate will decrease further, slowing the tank charging process. This effect causes the final stages of charging to last several hours. The predicted slowing effect is demonstrated in the profile of the average tank temperature during charging (Fig. 3).

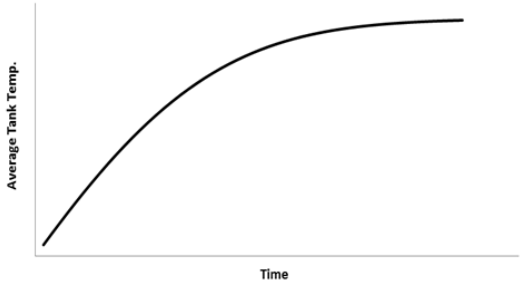

Fig. 3: Average Temperature profile within storage tank.

The thermosiphon flow over the entire process follows a bi-nodal profile (Fig. 4). As expected, the hydrostatic pressure will follow a similar profile to the thermosiphon flow rate. In order for a model to be considered successful, it must generate this bi-nodal flow profile under various system conditions.

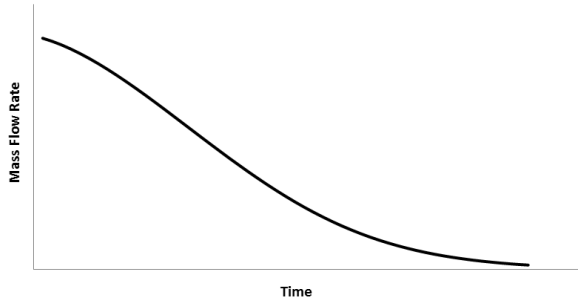

Fig. 4: Flow profile of a thermosiphon during storage tank charging.

MODEL DEVELOPMENT

In order for the model to be applied as a system design tool, it had to be developed around a first law analysis. The model was designed to account for the transient effects of natural convection flow rate, and to determine its impact on the charging of a storage tank. To determine this flow rate, Eq. 7 was used to find the pressure head in the heat exchanger loop and was balanced with the equation for total system loss based on the model by Lin et al. [5] (Eq. 8).

$$\oint \rho(T) g dz = \oint \rho(T) g dh_f \tag{8}$$

Since the flow in the storage tank will be very small, the friction losses in the tank were neglected. The pressure drop in the heat exchanger loop can then be written in terms of major and minor losses (Eq. 9).

$$\oint \rho(T) g dh_f = \Delta P_{hx} + \frac{\rho(T) V^2}{2}\left(f\frac{l}{d} + \zeta\right) \tag{9}$$

g is the gravitational constant, V is the velocity of the natural convection flow, f is the friction factor of the connecting pipe, l and d are the length and inner diameter of the connecting pipes respectively, and ΔP_{hx} is the pressure loss in the heat exchanger as given by Eq. 4, and ζ is the minor loss coefficient for the components used in the plumbing loop. Although the friction factor is normally a function of pipe roughness, at low flow rates (i.e., laminar) it is solely a function of the Reynold's Number [7] (Eq. 10).

$$f = \frac{64}{Re} \tag{10}$$

This allows the total closed path integral to be expressed in terms of the mass flow rate as well as known geometric conditions and fluid properties (Eq. 11).

$$\oint \rho(T) g dz = \Delta P_{hx}(\dot{m}_s) + \frac{128\mu(T) l \dot{m}_s}{\pi d^4 \rho(T)} + \frac{8\zeta}{\pi^2 \rho(\bar{T}) d^4}(\dot{m}_s)^2 \tag{11}$$

$\mu(T)$ is the kinematic viscosity of the water in the closed loop. To allow for the variation in temperature at the inlet and outlet of the heat exchanger, Eq. 11 was simplified to a sum of total pressure loss (Eq. 12).

$$\Delta P_{loss} = \Delta P_{hx} + \sum \Delta P_f + \sum \Delta P_m \tag{12}$$

ΔP_f is the friction losses in each of the pipe segments used in the system, and ΔP_m is the minor losses due to elbows, valves, and other componentry used in the system. The user of the simulation software is able to specify the total length of piping used in the proposed system, as well as any required componentry (e.g., elbows or other fittings). The pressure loss due to componentry is calculated using the generalized loss coefficient, ζ. This coefficient varies for each pipe component and was used when the pressure loss varies as a function of the mass flow rate (Eq. 13).

$$\Delta P_m = e * \zeta * m_s^2 \tag{13}$$

e is dependent on the diameter of the pipe, as well as the density of the fluid (see Eq. 11). This method of approximating minor losses with a generalized coefficient assumed a uniform increase in losses with an increase in mass flow rate.

In order to determine the characteristic equations required to size a BPHE (Eq. 4 and Eq. 5) the model was designed to use imported data from SWEP Int'l SSP G7 software [8]. This software contained many BPHE types in a variety of sizes and plate numbers. For each heat exchanger incorporated into the model, the performance characteristics were plotted and curve fitted in the form required by Eq. 4 and Eq. 5. Heat exchanger incorporation was limited to single-phase, between 10 and 20 plates. The heat transferred per unit of pressure drop degraded on either side of

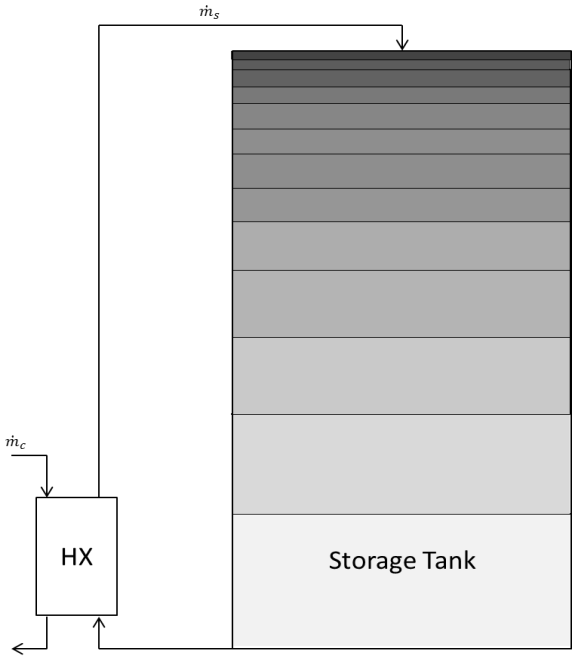

Fig. 5: Stratification profile within a storage tank.

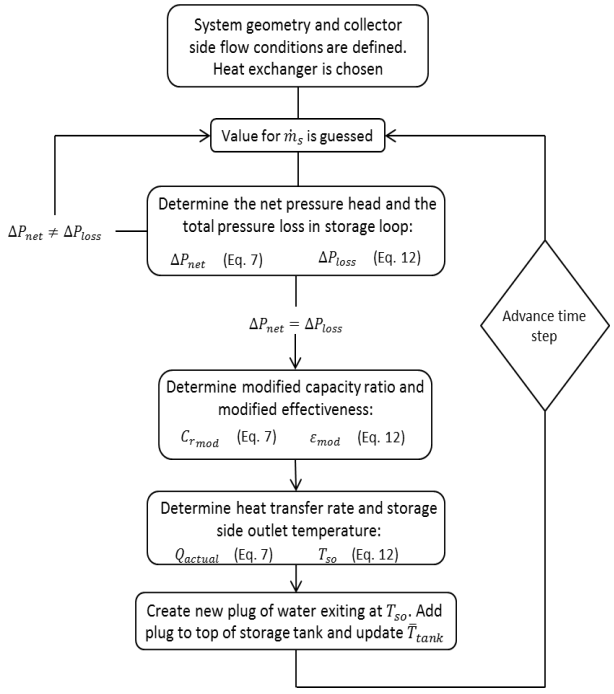

Fig. 6: Flow chart outlining model's iterative method.

this range. The system designer is able to select a heat exchanger for testing within the designed model, and the tank charging simulation will produce the performance indices for that specific configuration. A larger heat exchanger library can be attained with the addition of a dynamic-link library (DLL) from SWEP Int'l. This method would eliminate the need for the manual addition of performance indices and would reduce error due to curve fitting approximations.

The model that was created equates Eq. 7 and Eq. 11, and uses an iterative solver built into Microsoft Excel to solve for the mass flow rate at each time step. The model was designed to use a "plug" analysis (i.e., fixed volumes with constant properties) to replicate the effects of a stratifying storage tank with increasing temperatures and decreasing volumes (Fig. 5). These types of stratified tanks are especially effective in solar hot water systems with small temperature differences across the heat exchanger, relative to oil or gas heated tanks [9]. With each iteration, the average tank density decreased, causing a lower thermosiphon flow rate and thus a smaller plug to be added to the top of the storage tank. The lower flow rate also leads to a decrease in heat exchanger effectiveness and a consequent increase in the storage side exit temperature (Eq. 1). This process continued until the average tank density became too low to drive the flow. At this state, the storage tank was considered fully charged. Critical data can be exported from the model including total charging time, the tank temperature distribution, and the flow rate over the charging process. The iterative process that was used by the model can be seen in the flow chart (Fig. 6).

This process was repeated until the natural convection flow rate reaches 0.005 [LPM], which indicates that the thermosiphon has stalled and the tank is fully charged. After the simulation has been run, additional functionalities can be accessed to allow the system designer to have a better understanding of inherent thermosiphon characteristics. A temperature profile of the tank can be generated at any stage of the charging process to provide an accurate visual representation of the temperature distribution in the tank, as well as the actual sizes of water plugs being added (Fig. 7). Data for a specific test is saved to allow for comparison between heat exchangers or different system components. Additionally, the specification sheet is provided for the heat exchanger after each individual test.

As stated, the model was designed in Microsoft Excel, but was coded in Visual Basic for Applications (VBA). This method allows for many of the

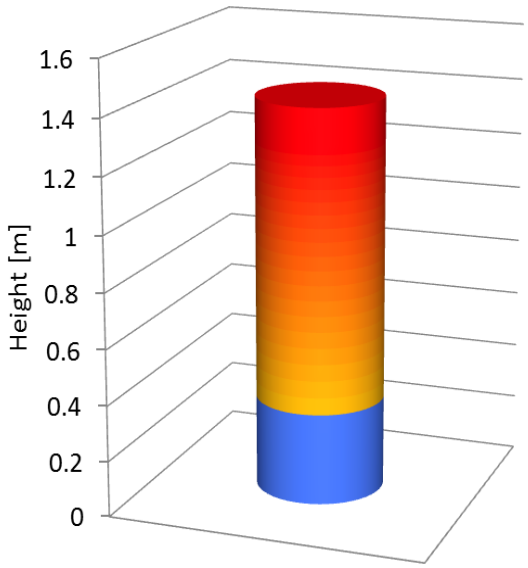

Fig. 7: Calculated storage tank temperature profile.

calculations to be completed outside of the spreadsheet, reducing the amount of processing power required for operation. Error handling was also included which prevents users from entering letters or nonsensical numbers that would result in errors or a system failure.

The model has several limitations due to some underlying assumptions that were made. The fluids within the system are assumed to have a constant specific heat. This will cause the heat transfer in the heat exchanger to vary slightly under high supply temperatures. It is also assumed that thermal effects are minimal inside the storage tank (i.e., no mixing of stratified layers and no heat loss to the environment). Adding a thermal loss would decrease the effectiveness of the model as a tool for designers, as additional tank specifications such as loss coefficients may not be available. Due to the complexity of plumbing systems, it is assumed that all piping used in the system will be the same diameter. This is often true for domestic purposes. Multi-diameter piping could be added, but would detract from the intuitive nature of the model.

APPARATUS

A full-scale test was carried out to determine the validity of the model and to assess the accuracy of the model's assumptions. The test apparatus that was used was based on the apparatus used by Purdy et al [2] (Fig. 8).

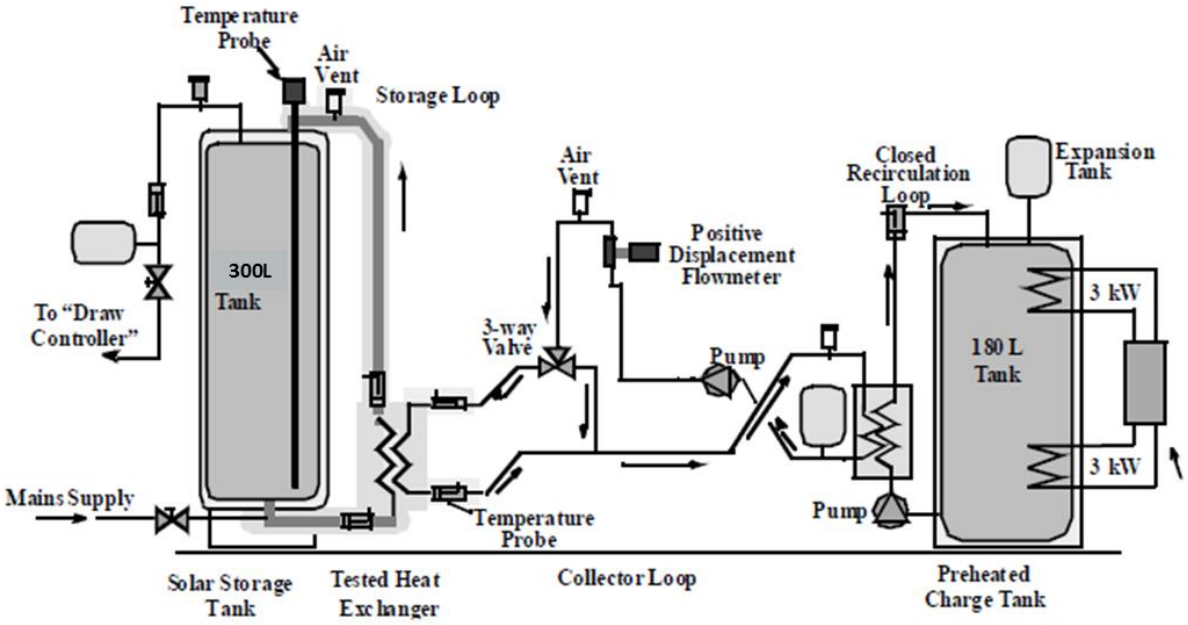

Fig. 8: Schematic of testing apparatus used in full-scale experiment

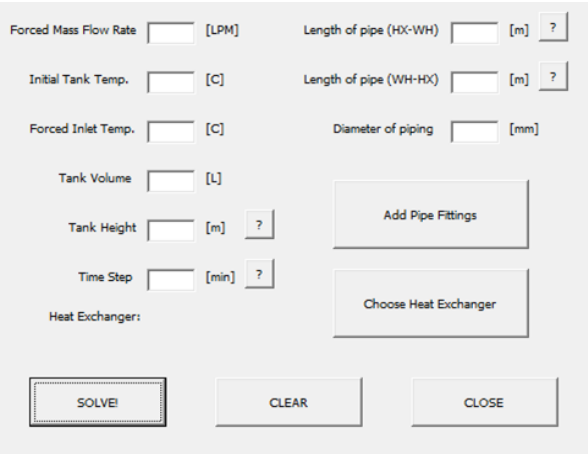

Fig. 9: Graphical user interface for entering data into model.

This configuration was proven effective in various studies [2], [5], [6]. The apparatus consisted of two hot water tanks and an externally mounted BPHE. A supply tank was used to simulate a solar thermal collection loop and was pre-heated prior to the start of the test. The heat input was transferred to the tested heat exchanger using a glycol/water mixture (50%-50% by volume) and was pumped through the collector side of the heat exchanger at a fixed flow rate. The supply fluid was kept at a constant temperature by a set-point temperature controller.

A 300L tank filled with potable water was used on the storage side of the heat exchanger loop. The system specifications and BPHE dimensions are seen in Table 1.

Table 1: System components and specifications.

Storage Tank	Steel Volume = 300 L Height = 1.3 m
Heat Exchanger	Brazed Plate Heat Exchanger B8T (20 Plates) Height = 0.317 m
Componentry	Total Pipe Length = 2.48 m Fittings = 8 x 90^o Elbow 2 x 45^o Elbow 2 x Branched-T 2 x Gate Valve (Open) Pipe Diameter = 12.7 mm

The componentry of the configuration as well as the heat exchanger type were also added to the model through a graphical user interface (GUI) (Fig. 9).

Any non-standard pipe components that were used, such as the flow meters, were approximated using other components in the GUI with similar pressure loss profiles.

EXPERIMENTAL METHOD

The experimental method that was used for data collection is as follows:

- Prior to testing, tanks were filled with their respective fluids.
- Supply tank was heated to a specified temperature.
- Both tanks were mixed to ensure a uniform temperature profile.
- Hot supply fluid was allowed to flow through the heat exchanger at a fixed rate.
- A computer based data-acquisition (D/A) system was turned on to record temperatures at 1 minute intervals at three ports of the heat exchanger and at 8 stratification levels within the storage tank. The fourth port was calculated empirically by the D/A system. Flow rates on both sides of the heat exchanger were also recorded.
- The supply loop conditions were maintained by a PID controller.
- Testing continued until the storage tank was fully charged, signified by an increase in temperature at the base of the tank. This event was verified by an increase in temperature at the inlet to the heat exchanger on the storage side.

Two tests were run using this configuration. The conditions for these test use the components outlined (Table 1) as well the parameters in Table 2.

Table 2: Temperatures and flow rates for tests.

Test Number	Forced-side Flow [LPM]	Forced-side Supply Temp.	Initial Tank Temp.
1	4.0	64	16
2	2.0	69	19

These test conditions are based on values that can be expected in a SDHW system, and were chosen to demonstrate the model's ability to account for slight

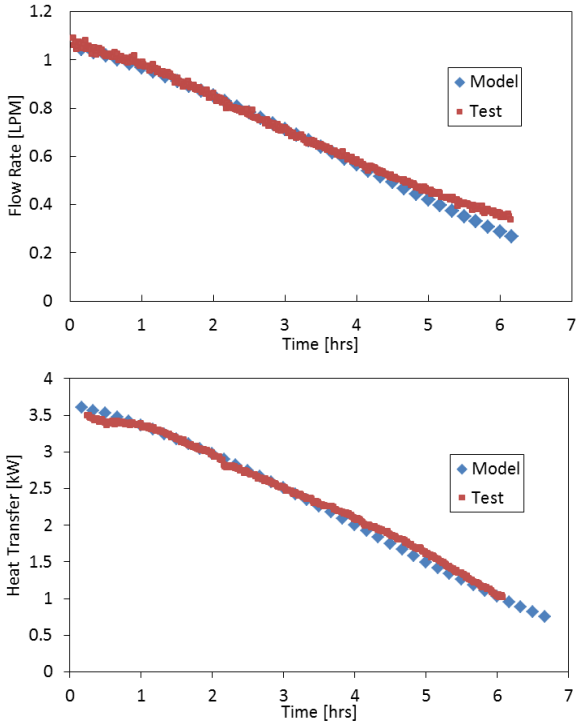

Fig. 10: Thermosiphon flowrate and heat transfer (Test 1).

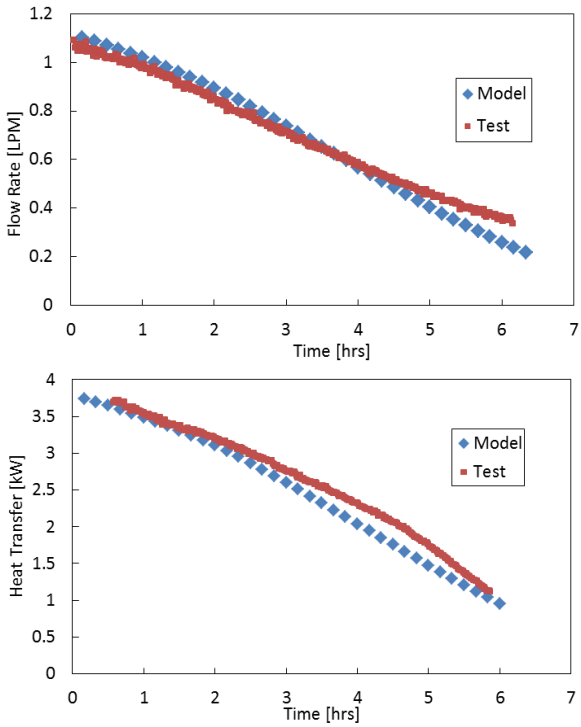

Fig. 11: Thermosiphon flowrate and heat transfer (Test 2).

variations in supply temperature and initial tank temperature.

RESULTS

The data from the experiment was compared to the predicted results from the model. The model calculated the natural convection mass flow rate over the charging of the storage tanks, as well as the heat transferred in the heat exchanger. In order to reduce the time needed to run the model, a ten minute time step was implemented. This time step was determined to be the fastest run time while producing accurate results with no aliasing. The experimental data was plotted against the model predictions for both system conditions (Fig. 10 and Fig. 11).

It can be seen that the model accurately predicts the bi-nodal shape of the flow rate, as well as the parabolic shape of the heat transfer during the charging process. It is also seen that the flow rates begin to diverge near the end of the charging process. This was due to the assumption of zero heat loss from the storage tank. As the test passed four hours, the large quantities of hot water began to lose heat to the surroundings, lowering the pressure head and prolonging the decrease in thermosiphon mass flow rate. Additionally, while the heat exchanger and plumbing were insulated, thermal losses still exist.

A calculation of the pressure head across the heat exchanger was made to ensure proper system operation. As expected, this pressure head across the heat exchanger matched the performance indices that were imported into the model (Eq. 4 and Eq. 5).

CONCLUSIONS

Natural convection heat exchanger systems are dependent on inherent conditions such as supply fluid flow rate, supply fluid temperature, and initial tank temperature. These conditions influence the average tank temperature and thus create the hydrostatic pressure head required to drive a thermosiphon.

A predictive model has been developed to simulate the charging of a natural convection DHW system under fixed conditions. A method has been created to account for the generalized pressure drop induced by system components. This allows designers to compare specific system designs and heat exchanger sections accounting for tank type, height, and the heat exchanger loop pressure drop. Designers may also compare a range of heat exchanger configurations regarding number of plates, heat transfer area, and

supply-side (i.e., forced flow) flow rates. This analysis allows the model to be employed by system designers on a large range of theoretical configurations to assess the viability of implementing a NCHE system.

The predictive model was able to accurately replicate a full-scale tank charging, producing accurate characteristic curves of thermosiphon flow rate and total heat transfer.

ACKNOWLEDGMENTS

The authors would like to thank the Canadian Natural Science and Engineering Research Council for supporting this work, as well as Christian Futschik and Kristen Jaczko for their assistance with apparatus construction and data acquisition.

REFERENCES

[1] F. Mauthner, W. Weiss, and S.-D. Monika, "Markets and Contributions to the Energy Supply 2013," *Int. Energy Agency*, p. 1, Jun. 2015.

[2] J. Purdy, S. Harrison, and P. H. Oosthuizen, "Thermal Evaluation of Compact Heat Exchangers in a Natural Convection Application," *Proc. 11th IHTC Heat Transf. 1998*, vol. 6, pp. 305–310, 1998.

[3] R. J. Cataford, *Effects of storage tank stratification on the performance of solar domestic hot water systems*. Kingston, Ont: Master's Thesis, 1995.

[4] K. F. Fraser, K. G. T. Hollands, and A. P. Brunger, "An empirical model for natural convection heat exchangers in SDHW systems," *Sol. Energy*, vol. 55, no. 2, pp. 75–84.

[5] Q. Lin, S. Harrison, and M. Lagerquist, "Analysis and Modelling of Compact Heat Exchangers for Natural Convection Application," presented at the EuroSun 2000, Copenhagen.

[6] C. Cruickshank and S. Harrison, "Experimental Characterization of a Natural Convection Hear Exchanger for Solar Domestic Hot Water Systems," in *Proceedings of ISEC 2006*, 2006.

[7] T. L. Bergman, F. P. Incropera, and A. S. Lavine, *Fundamentals of Heat and Mass Transfer*. John Wiley & Sons, 2011.

[8] *SSP G7 Simulation Software*. SWEP, 2015.

[9] N. Devore, H. Yip, and J. Rhee, "Domestic Hot Water Storage Tank: Design and Analysis for Improving Thermal Stratification," *J. Sol. Energy Eng.*, vol. 135, no. 4, pp. 040905–040905, Oct. 2013.